nature genetics

A suppressor screen in *Mecp2* mutant mice implicates cholesterol metabolism in Rett syndrome

Christie M Buchovecky[1], Stephen D Turley[2], Hannah M Brown[1,8], Stephanie M Kyle[1], Jeffrey G McDonald[3], Benny Liu[2], Andrew A Pieper[4,5,8], Wenhui Huang[6,8], David M Katz[7], David W Russell[3], Jay Shendure[6] & Monica J Justice[1]

Mutations in *MECP2*, encoding methyl CpG-binding protein 2, cause Rett syndrome, the most severe autism spectrum disorder. Re-expressing *Mecp2* in symptomatic *Mecp2*-null mice markedly improves function and longevity, providing hope that therapeutic intervention is possible in humans. To identify pathways in disease pathology for therapeutic intervention, we carried out a dominant *N*-ethyl-*N*-nitrosourea (ENU) mutagenesis suppressor screen in *Mecp2*-null mice and isolated five suppressors that ameliorate the symptoms of *Mecp2* loss. We show that a stop codon mutation in *Sqle*, encoding squalene epoxidase, a rate-limiting enzyme in cholesterol biosynthesis, underlies suppression in one line. Subsequently, we also show that lipid metabolism is perturbed in the brains and livers of *Mecp2*-null male mice. Consistently, statin drugs improve systemic perturbations of lipid metabolism, alleviate motor symptoms and confer increased longevity in *Mecp2* mutant mice. Our genetic screen therefore points to cholesterol homeostasis as a potential target for the treatment of patients with Rett syndrome.

Rett syndrome (RTT; MIM 312750) is an X-linked neurological disorder presenting with autistic features that afflicts approximately 1 in 10,000 females. After a few months or years of apparently normal postnatal development, progressive neurological manifestations of disease occur, including loss of speech and motor skills, stereotypic hand movements, difficulty walking, irregular breathing and seizures. Mutations in the X-linked gene *MECP2* are the primary cause of RTT[1]. Hemizygous males with truncating or loss-of-function mutations typically die of encephalopathy, whereas mild mutations in either sex are associated with a variety of intellectual disabilities and autism[2].

Mouse models recapitulate many of the symptoms of RTT, and their study has provided insight into the physiological basis of disease[3–5]. Although heterozygous female *Mecp2*/+ mice show phenotypic variance due in part to random X-chromosome inactivation, hemizygous male *Mecp2*/Y mice have a fully penetrant phenotype. *Mecp2*-null males are normal at birth and weaning but then develop limb clasping, tremors, lethargy and abnormal breathing, which progressively worsen until death between 6 and 16 weeks of age. Restoration of *Mecp2* expression in mutant mice after the onset of symptoms rescues the neurological deficits, including motor function, and significantly prolongs survival[6]. Therefore, MECP2 has roles in the postnatal maturation and/or maintenance of neuronal properties and circuits[4]. These findings suggest that RTT may be ameliorated or even reversed by genetic or pharmacological means after symptom onset[2,7]. Mechanistically, MECP2 binds to methylated DNA to regulate gene transcription through repression or activation[8]. When MECP2 represses gene transcription, it associates with chromatin-remodeling complexes that contain type I histone deacetylases (HDACs)[2,9]. As an epigenetic factor, MECP2 expression is therefore critical within a relatively narrow range, making gene therapy a difficult approach for symptom rescue.

We reasoned that a genetic screen for suppressors of symptoms using a *Mecp2* mouse model could identify pathways that are responsible for disease pathology and may thereby help pinpoint potential therapeutic targets. Genetic modifier screens are commonly applied to identify genes that act in developmental or biochemical pathways in fruit flies, worms and bacteria[10]; however, this approach is uncommon in mice[11,12]. Here we take advantage of advances in mutagenesis, sequencing and genotyping methods[13] to identify five loci that suppress disease phenotypes in *Mecp2*-null mice. One suppressing mutation occurs in *Sqle*, which encodes squalene epoxidase, a rate-limiting enzyme in cholesterol synthesis. Mutation of a rate-limiting enzyme such as SQLE suggests that downregulation of the cholesterol synthesis pathway can ameliorate symptoms. In support of this idea, we show that administration of statins, which also inhibit the cholesterol synthesis pathway, improves motor performance and increases longevity in *Mecp2* mutant mice. Cholesterol homeostasis may therefore be a therapeutic target for treating specific features of RTT pathology.

[1]Department of Molecular and Human Genetics, Baylor College of Medicine, Houston, Texas, USA. [2]Department of Internal Medicine, University of Texas Southwestern Medical School, Dallas, Texas, USA. [3]Department of Molecular Genetics, University of Texas Southwestern Medical School, Dallas, Texas, USA. [4]Department of Psychiatry, University of Texas Southwestern Medical School, Dallas, Texas, USA. [5]Department of Biochemistry, University of Texas Southwestern Medical School, Dallas, Texas, USA. [6]Department of Genome Sciences, University of Washington, Seattle, Washington, USA. [7]Department of Neurosciences, Case Western Reserve University School of Medicine, Cleveland, Ohio, USA. [8]Present addresses: Research Centre for Reproductive Health, School of Paediatrics and Reproductive Health, The University of Adelaide, Adelaide, South Australia, Australia (H.M.B.), Department of Psychiatry, University of Iowa Carver College of Medicine, Iowa City, Iowa, USA (A.A.P.), Department of Neurology, University of Iowa Carver College of Medicine, Iowa City, Iowa, USA (A.A.P.) and Fred Hutchinson Cancer Research Center, Seattle, Washington, USA (W.H.). Correspondence should be addressed to M.J.J. (mjustice@bcm.edu).

Received 12 February; accepted 24 June; published online 28 July 2013; doi:10.1038/ng.2714

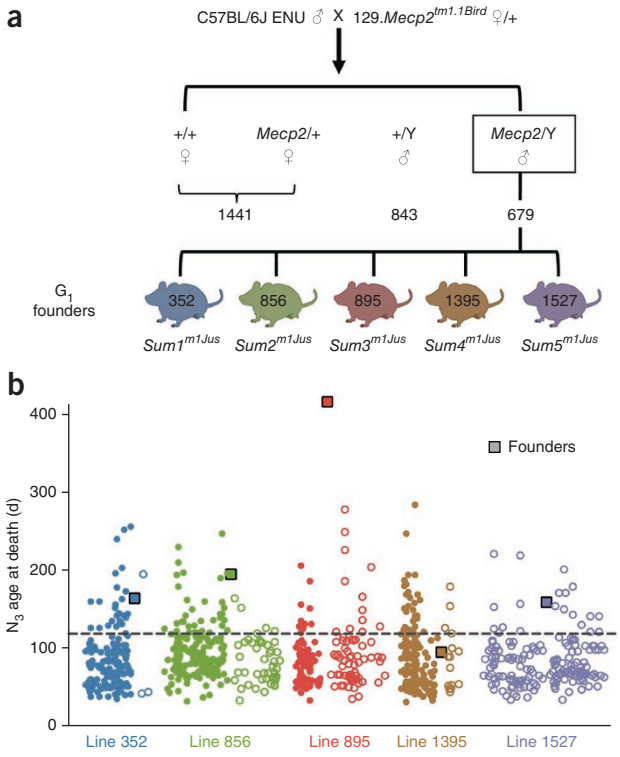

Figure 1 A dominant suppressor screen shows inheritance of longevity in five lines. (**a**) ENU-treated C57BL/6J males were mated to 129. *Mecp2*$^{tm1.1Bird}$/+ females. The G_1 *Mecp2*$^{tm1.1Bird}$/Y males (boxed) were aged and assessed for forelimb and hindlimb clasping, tremors, body size, cage activity and longevity. +/+, female wild-type mice; +/Y, male wild-type mice. (**b**) N_2 mice from five lines (352 (*Sum1*^{m1Jus}; blue), 856 (*Sum2*^{m1Jus}; green), 895 (*Sum3*^{m1Jus}; red), 1395 (*Sum4*^{m1Jus}; brown) and 1527 (*Sum5*^{m1Jus}; purple)) produced N_3 offspring that showed increased longevity. Closed circles represent offspring of a male N_2 parent, and open circles represent offspring of a female N_2 parent. The longevity of the G_1 founder of each line is indicated by the colored squares. *Mecp2*$^{tm1.1Bird}$/Y mice rarely survive past 120 d (horizontal dashed line).

RESULTS

ENU screen identifies five suppressors of *Mecp2*

We treated C57BL/6J male mice with ENU and mated them to female mice heterozygous for the Bird null allele of *Mecp2* made congenic on a 129S6/SvEv genetic background (129.*Mecp2*$^{tm1.1Bird}$/+) (**Fig. 1a**). We then screened first-generation (G_1) *Mecp2*-null males (*Mecp2*$^{tm1.1Bird}$/Y) for rescue of neurological defects using a health scoring system that included assessments of limb clasping, tremors, body size, cage activity and development of skin and/or eye inflammation or malocclusion. Of 2,963 G_1 mice weaned, 1,522 were male and 679 were *Mecp2*$^{tm1.1Bird}$/Y. Most of the G_1 *Mecp2*$^{tm1.1Bird}$/Y mice had mild neurological abnormalities by 4 weeks of age and died or had to be euthanized by 6–16 weeks of age; however, some of these mice showed amelioration of one or more of the health assessment traits. These 25 males were placed in mating cages to assess heritability and longevity caused by a putative second-site mutation; litters were obtained from seven of the mice. Five lines showed inherited suppressor loci, which we named suppressor of *Mecp2* mutations 1–5 (*Sum1*^{m1Jus}, MGI 5489912; *Sum2*^{m1Jus}, MGI 5489913; *Sum3*^{m1Jus}, MGI 5489914; *Sum4*^{m1Jus}, MGI 5489915; and *Sum5*^{m1Jus}, MGI 5489916; **Fig. 1b**). Each suppressor showed different degrees of health-trait rescue (**Table 1** and **Supplementary Fig. 1**); however, all suppressors increased the lifespan of *Mecp2*/Y mice by at least 3 weeks from the average 50% lethality time point. Each survival curve showed a characteristic pattern that reflected the manifestation of health traits (**Fig. 2**). Two male mice, 352 (*Sum1*^{m1Jus}) and 1395 (*Sum4*^{m1Jus}), showed rescue of multiple traits, even though they did not live particularly long lives (163 and 94 d, respectively). Both of these mice died suddenly without showing *Mecp2*-null symptoms, but each founded lines in which the offspring lived much longer, highlighting the predictive nature of neurological and health assessments on longevity. Unexpected phenotypes emerged in some of the lines, which compromised the health of the mice. Long-lived *Mecp2*/Y mice from four of the lines, excluding *Sum1*^{m1Jus}, developed varying degrees of dermatitis, eye inflammation or malocclusions at different ages (**Table 1**). Inflammation is a key manifestation of *Mecp2* mutation in non-neural cells[14]. The rescue of different traits and the varying penetrance of phenotypes in rescue mice suggests that the mutations are suppressing through multiple mechanisms.

To identify a chromosomal location for the suppressing traits (where *M* is an unknown ENU-induced suppressing mutation), DNA from 7–12 long-lived *Mecp2*$^{tm1.1Bird}$/Y; *M*/+ mice from each founder line were genotyped along with DNA from short-lived *Mecp2*$^{tm1.1Bird}$/Y; +/+ N_3 littermates using an Illumina medium-density SNP panel. We analyzed the resulting genotypes for heterozygous C57BL/6J linkage to the rescue phenotype according to haplotype assessment at the N_3 generation[15,16]. These data showed significant linkage for *Sum1*^{m1Jus} on mouse chromosome 16 ($\log_{10}$ odds (LOD) score, 4.82), for *Sum2*^{m1Jus} on chromosome 3 (LOD score, 3.61), for *Sum3*^{m1Jus} on chromosome 15 (LOD score, 3.03) and for *Sum4*^{m1Jus} on chromosome 7 (LOD score, 3.40) (**Supplementary Fig. 2a–d**). We confirmed linkage and achieved fine mapping by assessing markers within the putative map location for additional mice in the line (**Supplementary Fig. 3a–d**). The maximum LOD score for *Sum5*^{m1Jus} was 2.86; we did not confirm a map location in this line.

A stop-codon mutation confers rescue

We subjected genomic DNA from two third-generation *Mecp2*$^{tm1.1Bird}$/Y; *Sum3*^{m1Jus}/+ long-lived mouse cousins to exome capture and massively parallel sequencing[17]. We found seven heterozygous, protein-altering variants in both mice but not in 15 control mouse exomes (a set including C57BL/6J and 129S6/SvEvTac DNAs; **Supplementary Fig. 4a**).

Table 1 Subjective health scores averaged for offspring assessed in various lines

	Mecp2$^{tm1.1Bird}$/Y; *Sum1*^{m1Jus}/+		*Mecp2*$^{tm1.1Bird}$/Y; *Sum2*^{m1Jus}/+		*Mecp2*$^{tm1.1Bird}$/Y; *Sum3*^{m1Jus}/+		*Mecp2*$^{tm1.1Bird}$/Y; *Sum4*^{m1Jus}/+		*Mecp2*$^{tm1.1Bird}$/Y; *Sum5*^{m1Jus}/+		*Mecp2*$^{tm1.1Bird}$/Y; +/+	
Age (weeks)	8	20	8	20	8	20	8	20	8	20	8	20
Clasping	0	2	1	3	1	3	2	2	1	2	4	N/A
Tremors	0	1	1	1	1	2	2	2	1	2	3	N/A
Body weight	0	0	0	2	1	1	0	0	1	2	3	N/A
Lethargy	0	1	0	1	0	1	0	1	1	2	4	N/A
Inflammation	0	0	D, E	D, E	0	D	D	D, E	E	E	0	N/A
Malocclusion	0	–	0	–	1	–	1	–	0	–	1	–

Shown are the average health scores for each parameter at 8 and 20 weeks of age. The health scores are as follows: 0, not present; 1, normal and similar to wild type; increasing to 5, near death and warranting euthanasia. D, dermatitis; E, eye inflammation. N/A, not applicable, as *Mecp2*-null males do not live to this age.

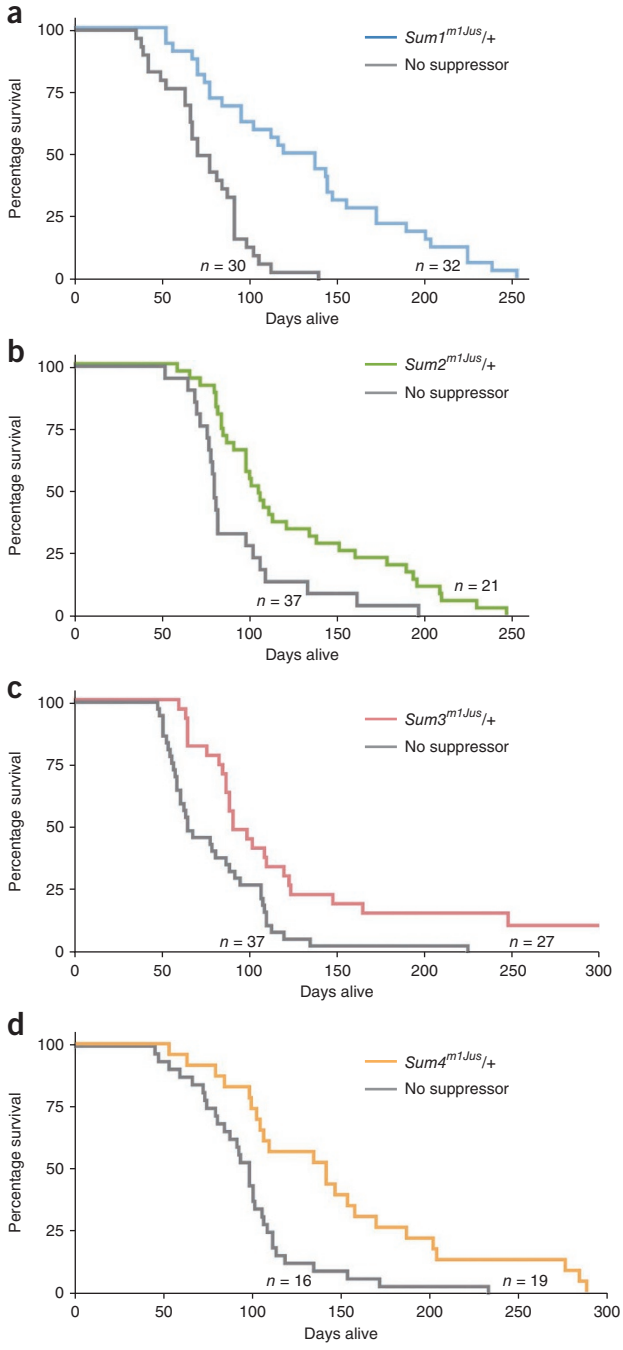

Figure 2 Survival curves for each line with a confirmed map location for the modifier are shown assessed at the N_3 generation. (**a**–**d**) Survival of *Mecp2*$^{tm1.1Bird}$/Y mice is significantly increased by the presence of each suppressing mutation in lines 352 (*Sum1*^{m1Jus}; $P = 0.001$) (**a**), 856 (*Sum2*^{m1Jus}; $P = 0.005$) (**b**), 895 (*Sum3*^{m1Jus}; $P = 0.002$) (**c**) and 1395 (*Sum4*^{m1Jus}; $P = 0.016$) (**d**). (Kaplan-Meier analysis followed by log-rank comparisons.)

Only one of these variants ranked highly with respect to both overlap with *Sum3*^{m1Jus}/+ mapping data (chromosome 15: 34260887–95144876; **Supplementary Fig. 4b**) and predicted functional impact: a nonsense mutation (c.1195C>T, p.Arg399X) in *Sqle* (ENSMUSG00000022351), encoding squalene epoxidase, also known as squalene monooxygenase (**Fig. 3a**).

SQLE catalyzes the first oxygenation reaction in the committed production of cholesterol, an essential lipid either supplied by diet or synthesized from acetate by a complex pathway[18,19]. Cholesterol homeostasis is maintained by negative feedback regulation of genes and their encoded enzymes in the pathway, including the rate-limiting enzymes 3-hydroxy-3-methylglutaryl–coenzyme A (HMG-CoA) reductase (HMGCR) and SQLE[20–22]. The enzymatic reaction of SQLE requires a mitochondrial electron donor to produce 2,3-oxidosqualene, a transient intermediate that is cyclized to lanosterol by lanosterol synthase (LSS)[23]. SQLE is expressed in many tissues[24] and is conserved throughout evolution; the mouse and human proteins are 84% identical at the amino acid level. Mice homozygous for *Sqle*^{Sum3Jus} die before birth at embryonic day (E) 8.5, a phenotype that is consistent with that found in other mice with mutations affecting cholesterol synthesis[25] (**Supplementary Table 1**). Two isoforms are annotated in mice: the *Sqle*^{Sum3Jus} stop mutation identified here occurs in a highly conserved exon present in the long isoform, which, unlike the short isoform, is consistently translated to protein in mammalian species. The long isoform is absent in homozygous mutant *Sqle*^{Sum3Jus}/*Sqle*^{Sum3Jus} embryos, suggesting nonsense-mediated RNA decay, and the predicted short form is not upregulated in *Sqle*^{Sum3Jus}/*Sqle*^{Sum3Jus} embryos or *Sqle*^{Sum3Jus}/+ mice (**Fig. 3b** and **Supplementary Fig. 5**). Protein blot analysis of E8.0 *Sqle*^{Sum3Jus} homozygous embryos showed that the expected 64-kDa protein was absent, as was a 36-kDa presumed degradation product, which is consistent with a null mutation (**Fig. 3c**). Only one other null eukaryotic mutation of *Sqle* has been identified, which results in an inability of plants to tolerate drought stress[26,27].

Cholesterol synthesis takes place through complex pathways, all of which use the rate-limiting enzymes HMGCR and SQLE[28]. Previous analysis suggested that expression of *Hmgcr* and *Sqle* was predictive of the behavior of genes encoding intermediate enzymes in these pathways (data not shown). To determine the effect of the *Sqle* mutation on cholesterol biosynthesis, we assessed the expression of *Hmgcr* and *Sqle* in the brains and livers of *Sqle*^{Sum3Jus}/+ mice (**Fig. 3d**,**e**). *Sqle* expression was reduced by nearly 50% in *Sqle*^{Sum3Jus}/+ brains at P70, with no compensatory change in *Hmgcr* expression (**Fig. 3d** and **Supplementary Table 2**). *Sqle* expression was also reduced in the brains of 129.*Mecp2*$^{tm1.1Bird}$/Y mice regardless of *Sqle*^{Sum3Jus} mutation status. Consistently, concentrations of the cholesterol precursors desmosterol and lanosterol were decreased in *Sqle*^{Sum3Jus}/+ brains at P70 (**Fig. 3f** and **Supplementary Table 3a**). Livers of *Sqle*^{Sum3Jus}/+ mice at P70 showed little decrease in *Sqle* or *Hmgcr* expression, although the 129.*Mecp2*$^{tm1.1Bird}$/Y mice had increased expression of both genes regardless of *Sqle*^{Sum3Jus} mutation status (**Fig. 3e**). Likewise, these changes in expression are reflected in serum cholesterol concentrations (**Fig. 3g**). Together these data suggest that *Sqle*^{Sum3Jus}/+ mice carry a loss-of-function allele of *Sqle*.

To determine which RTT-like traits were ameliorated in 129.*Mecp2*$^{tm1.1Bird}$/Y; *Sqle*^{Sum3Jus}/+ mice, we carried out a series of behavioral and breathing assessments out at the N_7 backcross generation. In addition to increased longevity, these mice showed improved motor activity on a rotarod (**Fig. 3h**) and increased activity in the open field (**Fig. 3i**). However, they showed little improvement of irregular respiration as measured by plethysmography and no change in acoustic startle responses (**Supplementary Fig. 6a–d**). Thus, heterozygous loss of *Sqle* does not improve all the symptoms that are associated with *Mecp2* mutation.

Mecp2-null male mice have abnormal cholesterol metabolism

We hypothesized that the heterozygous *Sqle* mutation ameliorates a previously unrecognized dysregulation of cholesterol metabolism in *Mecp2*-null mice. Cholesterol is a major and essential component of the brain, which must be produced there exclusively through synthesis, as cholesterol-rich lipoproteins cannot cross the

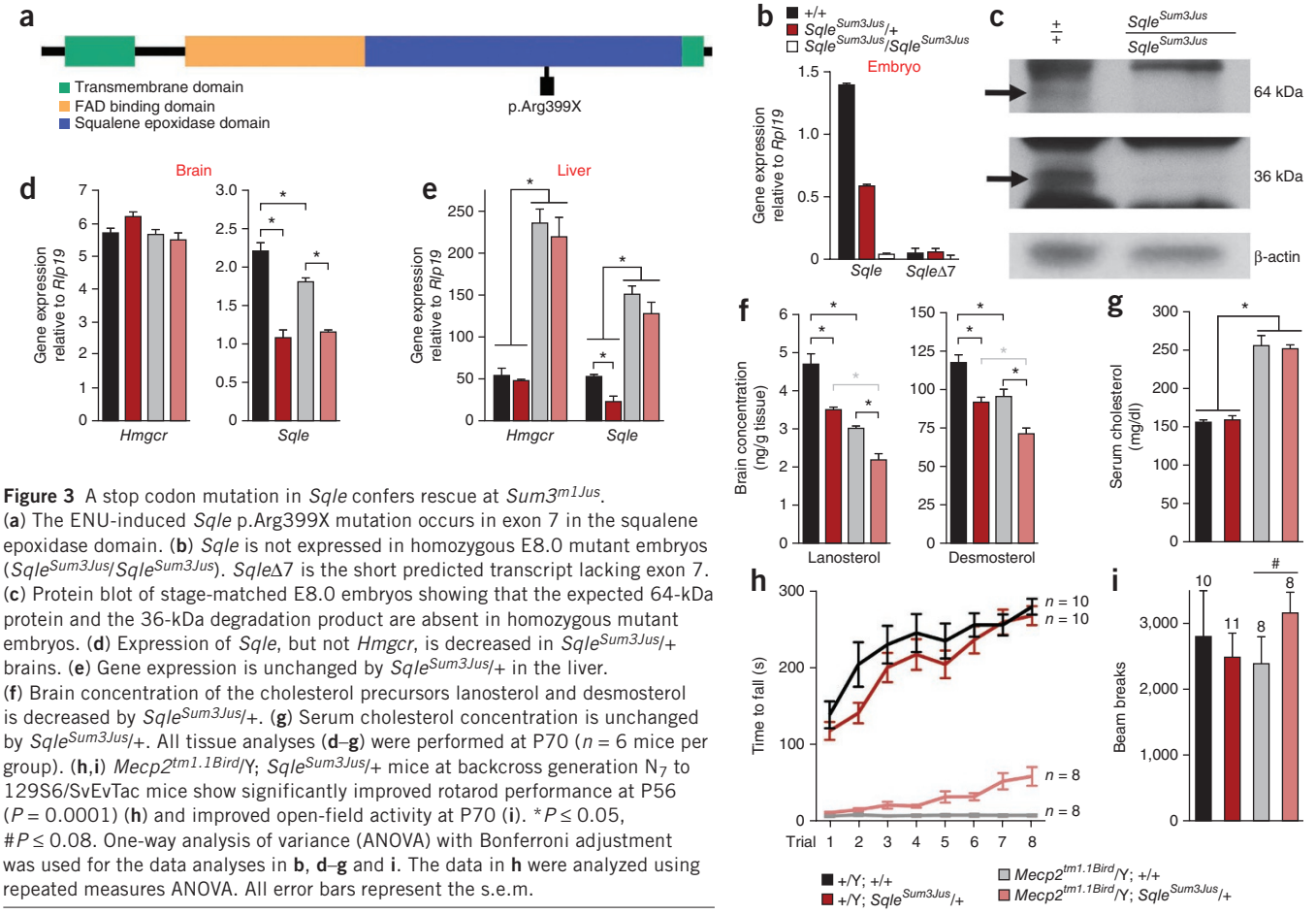

Figure 3 A stop codon mutation in *Sqle* confers rescue at *Sum3*^{m1Jus}. (**a**) The ENU-induced *Sqle* p.Arg399X mutation occurs in exon 7 in the squalene epoxidase domain. (**b**) *Sqle* is not expressed in homozygous E8.0 mutant embryos (*Sqle*^{Sum3Jus}/*Sqle*^{Sum3Jus}). *Sqle*Δ7 is the short predicted transcript lacking exon 7. (**c**) Protein blot of stage-matched E8.0 embryos showing that the expected 64-kDa protein and the 36-kDa degradation product are absent in homozygous mutant embryos. (**d**) Expression of *Sqle*, but not *Hmgcr*, is decreased in *Sqle*^{Sum3Jus}/+ brains. (**e**) Gene expression is unchanged by *Sqle*^{Sum3Jus}/+ in the liver. (**f**) Brain concentration of the cholesterol precursors lanosterol and desmosterol is decreased by *Sqle*^{Sum3Jus}/+. (**g**) Serum cholesterol concentration is unchanged by *Sqle*^{Sum3Jus}/+. All tissue analyses (**d**–**g**) were performed at P70 ($n = 6$ mice per group). (**h**,**i**) *Mecp2*$^{tm1.1Bird}$/Y; *Sqle*^{Sum3Jus}/+ mice at backcross generation N_7 to 129S6/SvEvTac mice show significantly improved rotarod performance at P56 ($P = 0.0001$) (**h**) and improved open-field activity at P70 (**i**). $^*P \leq 0.05$, $\#P \leq 0.08$. One-way analysis of variance (ANOVA) with Bonferroni adjustment was used for the data analyses in **b**, **d**–**g** and **i**. The data in **h** were analyzed using repeated measures ANOVA. All error bars represent the s.e.m.

blood-brain barrier[29]. To facilitate proper neurotransmitter release and dendrite remodeling, neuronal membranes require constant turnover to eliminate cholesterol that has been adulterated by reactive oxygen species, which are byproducts of their high rate of metabolism[30]. When neurons require cholesterol turnover or accumulate too much cholesterol or its intermediates, the cytochrome P450 oxidase Cyp46a1 hydroxylates cholesterol to produce 24*S*-hydroxycholesterol, allowing for egress by one-way diffusion into the circulation across the blood-brain barrier (**Fig. 4a**)[31]. Two alleles of *Mecp2* are primarily used as mouse models of RTT: *Mecp2*$^{tm1.1Bird}$, a null mutation[3], and *Mecp2*$^{tm1.1Jae}$, which expresses low levels of a truncated protein[32]. At postnatal day (P) 28, when *Mecp2*/Y mice show mild symptoms, *Cyp46a1* expression was increased 38% in 129.*Mecp2*$^{tm1.1Bird}$/Y brains over wild-type brains ($P = 0.02$), with a similar trend seen in B6.*Mecp2*$^{tm1.1Jae}$/Y brains, indicating a heightened need for cholesterol turnover by neurons in the early stages of disease (**Fig. 4b**). Notably, brains carrying the two different *Mecp2* alleles also showed higher concentrations of total cholesterol at P56 (129.*Mecp2*$^{tm1.1Bird}$/Y, $P = 0.05$; B6.*Mecp2*$^{tm1.1Jae}$/Y, $P = 0.21$; **Fig. 4c**). However, by P56, when mutant male mice are severely symptomatic, the cholesterol biosynthesis and turnover genes *Hmgcr*, *Sqle* and *Cyp46a1* were downregulated in both alleles (**Fig. 4b**). Desmosterol is the most prevalent intermediate that is produced by the primary cholesterol synthesis pathway in the adult brain[33]. Notably, the amount of desmosterol was also decreased at P56 in 129.*Mecp2*$^{tm1.1Bird}$/Y brains ($P = 0.01$), and the amounts of both lanosterol and desmosterol were decreased by P70. Furthermore, by P70, brain cholesterol concentrations had returned to wild-type levels, reflecting cholesterol biosynthesis pathway downregulation in the adult 129.*Mecp2*$^{tm1.1Bird}$/Y brain (**Fig. 4c** and **Supplementary Table 3a**,**b**). Similarly, *de novo* cholesterol synthesis assayed by the *in vivo* incorporation of ^3H_2O into sterols[34] confirmed that sterol synthesis decreased in the adult brains of B6.*Mecp2*$^{tm1.1Jae}$/Y mice (**Fig. 4d** and **Supplementary Table 4a**,**b**). Therefore, brain cholesterol metabolism is perturbed in two *Mecp2* alleles on two different genetic backgrounds. Either increased or decreased amounts of sterols can impair neurological function, demanding a tight regulation of brain sterol synthesis[35]. In *Mecp2* mutant mice, our data suggest that overproduction of cholesterol in the brain probably feeds back to decrease synthesis.

Although RTT is primarily a neurological disease, most cholesterol synthesis studies have been carried out in the liver, which regulates the systemic release of cholesterol in conjunction with dietary consumption. The expression of *Hmgcr and Sqle* was unchanged at P28 and was significantly higher at P56 in 129.*Mecp2*$^{tm1.1Bird}$/Y livers compared to wild-type livers ($P \leq 0.05$; **Fig. 4e**). Although total liver cholesterol and phospholipid concentrations were unchanged, reflecting the transient nature and rapid packaging of newly synthesized cholesterol into lipoproteins for secretion, the concentration of the primary liver-storage lipids, triacylglycerides (TAGs), was greatly increased in 129.*Mecp2*$^{tm1.1Bird}$/Y mice by P56 ($P = 0.003$; **Fig. 4f** and **Supplementary Fig. 7**). In contrast, B6.*Mecp2*$^{tm1.1Jae}$ mice showed no significant perturbations in gene expression at P28 or P56, a modest increase in *de novo* liver cholesterol synthesis and a modest increase in liver TAG concentration at P56 (**Fig. 4e**–**g** and **Supplementary Table 4a**,**b**). Consistently, total serum cholesterol, low-density lipoprotein (LDL) cholesterol and triglyceride concentrations were significantly elevated in 129.*Mecp2*$^{tm1.1Bird}$/Y mice ($P \leq 0.01$), but not

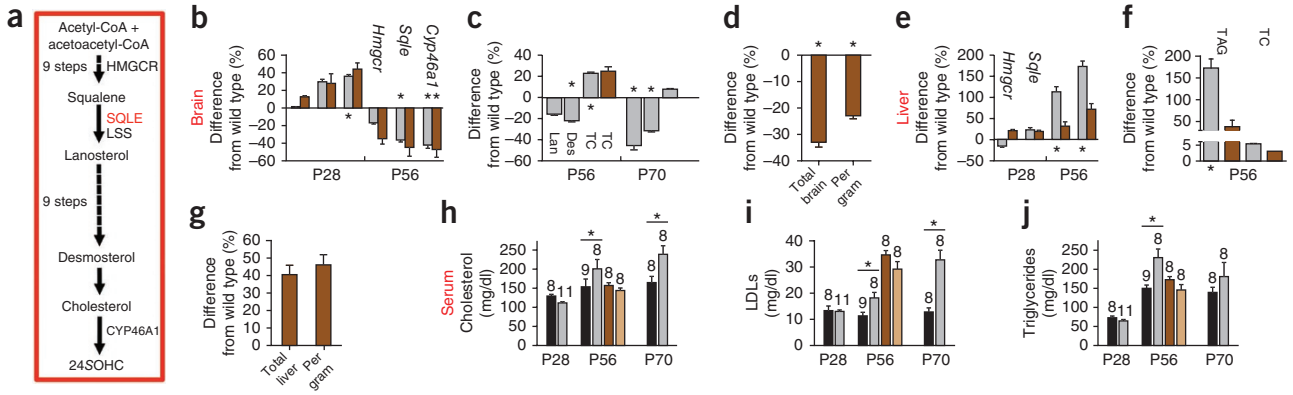

Figure 4 Cholesterol metabolism is disrupted in *Mecp2*-null male mice. (**a**) A simplified schematic of the enzymes and products in cholesterol biosynthesis through desmosterol is shown. (**b**) Expression of *Hmgcr*, *Sqle* and *Cyp46a1* is similar in the brains of *Mecp2*$^{tm1.1Bird}$/Y and *Mecp2*$^{tm1.1Jae}$/Y mice. (**c**) Lanosterol (Lan), desmosterol (Des) and total cholesterol (TC) concentrations are shown per gram of brain tissue at P56 ($n = 8$ mice per group) and P70 ($n = 4$ mice per group). (**d**) Cholesterol synthesis is decreased in *Mecp2*$^{tm1.1Jae}$/Y brains at P56 (wild type, $n = 4$; null, $n = 5$). (**e**) Expression of *Hmgcr* and *Sqle* differs in the livers of *Mecp2*$^{tm1.1Bird}$/Y and *Mecp2*$^{tm1.1Jae}$/Y mice. (**f**) Triacylglyceride (TAG) and total cholesterol concentrations are shown per gram of liver tissue at P56 ($n = 6$ mice per group). (**g**) Cholesterol synthesis is slightly increased in *Mecp2*$^{tm1.1Jae}$/Y livers per gram of tissue at P56 (wild type, $n = 4$; null, $n = 5$). In **b**–**g**, gray represents the *Mecp2*$^{tm1.1Bird}$ line, and brown represents the *Mecp2*$^{tm1.1Jae}$ line. (**h**–**j**) Total cholesterol (**h**), LDL cholesterol (**i**) and triglyceride (**j**) concentrations in serum are significantly higher in *Mecp2*$^{tm1.1Bird}$/Y mice by P56 but are unchanged in *Mecp2*$^{tm1.1Jae}$/Y mice ($n = 6$ mice per group). In **h**–**j**, black represents 129 +/Y mice, brown represents B6 +/Y mice, gray represents 129.*Mecp2*$^{tm1.1Bird}$/Y mice, and light tan represents B6.*Mecp2*$^{tm1.1Jae}$/Y mice. For the gene expression data in **b** and **e**, $n = 6$ mice per genotype at P28 and 12 mice per genotype at P56 for *Mecp2*$^{tm1.1Bird}$, and $n = 4$ mice per genotype at P28 and 6 mice per genotype at P56 for *Mecp2*$^{tm1.1Jae}$. Tissue data (**b**–**g**) show the percentage change from wild-type levels. $^*P \leq 0.05$. Statistical analyses were performed using Student's *t* test. All error bars represent the s.e.m.

B6.*Mecp2*$^{tm1.1Jae}$/Y mice, at P56 (**Fig. 4h**–**j**). The C57BL/6J inbred strain and the 129/Sv substrains inherently manage peripheral cholesterol metabolism differently[36]. Together these data suggest that perturbations in brain cholesterol synthesis are common in the two alleles in two different strain backgrounds; however, severe peripheral dysregulation of the pathway occurs only in the 129.*Mecp2*$^{tm1.1Bird}$ strain.

Statins ameliorate behavioral and metabolic symptoms

Aberrant cholesterol metabolism may therefore contribute to *Mecp2*-null symptoms. We reasoned that a pharmacologic inhibitor of cholesterol synthesis might produce an attenuation of symptoms comparable to that of the genetic inhibitor *Sqle*^{Sum3Jus}/+ in *Mecp2*-null mice. We treated wild-type and 129.*Mecp2*$^{tm1.1Bird}$/Y mutant mice with statin drugs, which are commonly prescribed to reduce systemic cholesterol by interfering with cholesterol synthesis through competitive inhibition of HMGCR. As a preliminary trial, we treated age-matched littermates with 3 mg per kg body weight of fluvastatin weekly starting at 5 weeks of age. This treatment lowered serum cholesterol concentrations and increased cage activity during a 3-week trial period (data not shown). Starting at week 8, we increased administration of the 3 mg per kg body weight dose of fluvastatin to three times per week (**Supplementary Table 5**). Fluvastatin treatment lowered serum

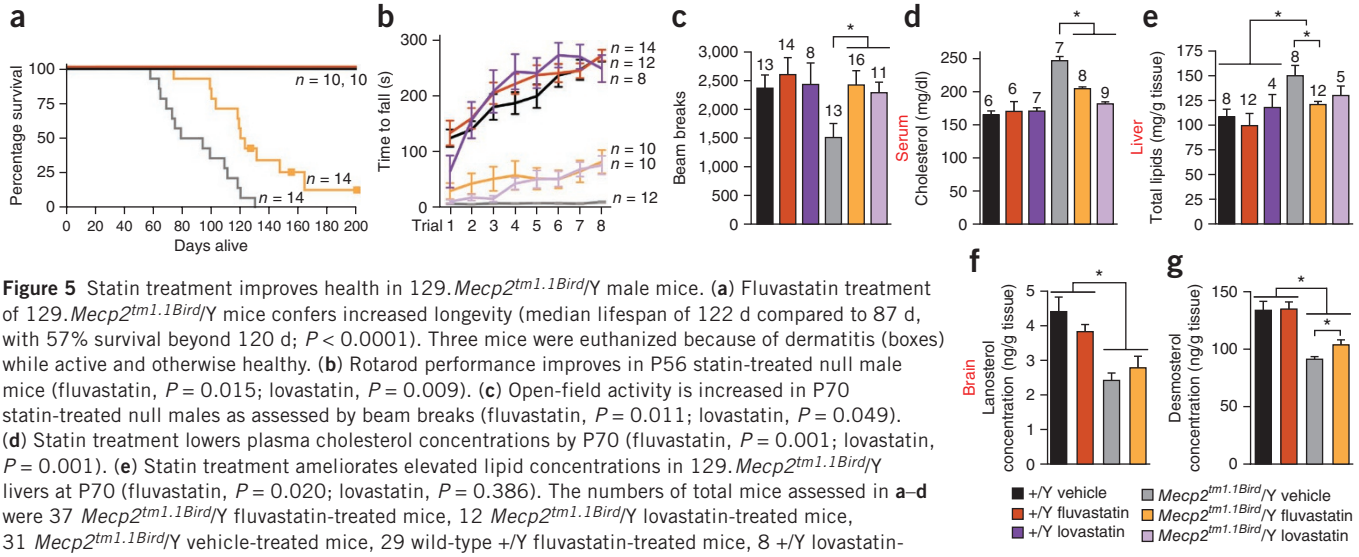

Figure 5 Statin treatment improves health in 129.*Mecp2*$^{tm1.1Bird}$/Y male mice. (**a**) Fluvastatin treatment of 129.*Mecp2*$^{tm1.1Bird}$/Y mice confers increased longevity (median lifespan of 122 d compared to 87 d, with 57% survival beyond 120 d; $P < 0.0001$). Three mice were euthanized because of dermatitis (boxes) while active and otherwise healthy. (**b**) Rotarod performance improves in P56 statin-treated null male mice (fluvastatin, $P = 0.015$; lovastatin, $P = 0.009$). (**c**) Open-field activity is increased in P70 statin-treated null males as assessed by beam breaks (fluvastatin, $P = 0.011$; lovastatin, $P = 0.049$). (**d**) Statin treatment lowers plasma cholesterol concentrations by P70 (fluvastatin, $P = 0.001$; lovastatin, $P = 0.001$). (**e**) Statin treatment ameliorates elevated lipid concentrations in 129.*Mecp2*$^{tm1.1Bird}$/Y livers at P70 (fluvastatin, $P = 0.020$; lovastatin, $P = 0.386$). The numbers of total mice assessed in **a**–**d** were 37 *Mecp2*$^{tm1.1Bird}$/Y fluvastatin-treated mice, 12 *Mecp2*$^{tm1.1Bird}$/Y lovastatin-treated mice, 31 *Mecp2*$^{tm1.1Bird}$/Y vehicle-treated mice, 29 wild-type +/Y fluvastatin-treated mice, 8 +/Y lovastatin-treated mice and 29 wild-type +/Y vehicle-treated mice. (**f**,**g**) The concentration of lanosterol slightly increases (**f**) and that of desmosterol significantly increases (**g**) in the brains of fluvastatin-treated 129.*Mecp2*$^{tm1.1Bird}$/Y mice at P70 ($n = 4$ mice per group; $P = 0.042$). The data in **b** were analyzed using repeated measures ANOVA. One-way ANOVA was used for the data analyses in **c**–**g**. $^*P \leq 0.05$ determined using Dunnett's *post-hoc* test to compare statin- with vehicle-treated groups. All error bars represent the s.e.m.

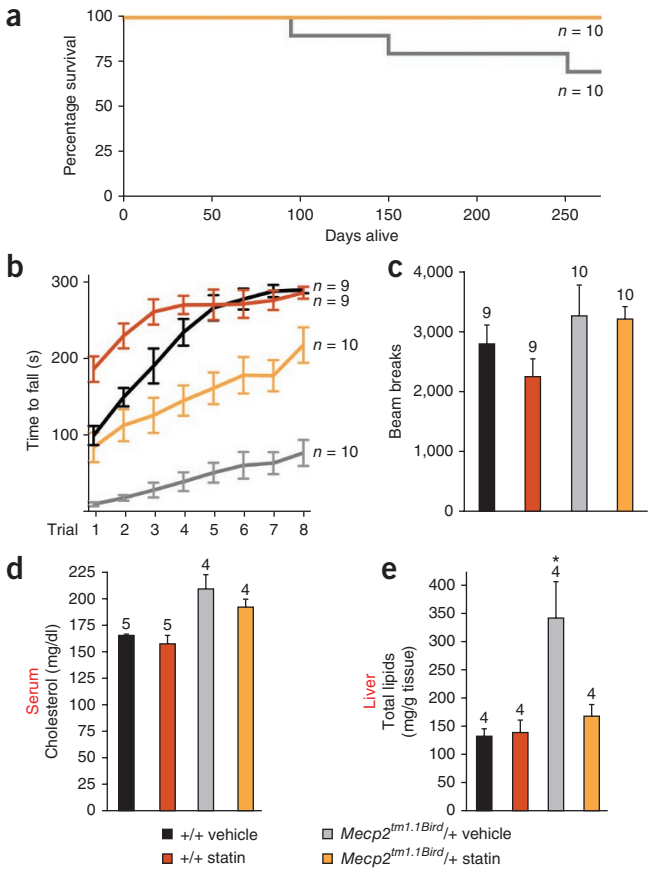

Figure 6 Fluvastatin treatment improves health in 129.*Mecp2*$^{tm1.1Bird}$/+ female mice. (**a**) No fluvastatin-treated 129.*Mecp2*$^{tm1.1Bird}$/+ female mice died before 8 months of age, but three vehicle-treated female mice died. (**b**) Rotarod performance improves in 5-month-old fluvastatin-treated 129.*Mecp2*$^{tm1.1Bird}$/+ female mice ($P = 0.001$). (**c**) Open-field activity assessed at 4 months of age shows no significant differences in the fluvastatin- and vehicle-treated groups. (**d**) Fluvastatin treatment does not significantly change serum cholesterol concentrations at 8 months of age. (**e**) Fluvastatin treatment ameliorates elevated lipid concentrations in 129.*Mecp2*$^{tm1.1Bird}$/+ livers assessed at 8 months of age ($^*P = 0.045$). The data in **b** were analyzed using repeated measures ANOVA. One-way ANOVA was used for the data analyses in **c**–**e**. $^*P \leq 0.05$ determined using Dunnett's *post-hoc* test to compare statin- with vehicle-treated groups. All error bars represent the s.e.m.

cholesterol and total liver lipids, improved subjective health scores, rotarod performance and open-field activity and increased lifespan when compared with control mice receiving a sham dose (**Fig. 5a**–**e**) and was more effective at improving these parameters than the *Sqle* mutation. Similar to the *Sqle* mutation, fluvastatin treatment did not improve baseline breathing irregularity or acoustic startle responses (**Supplementary Fig. 8a**–**d**).

Markedly, brains of fluvastatin-treated 129.*Mecp2*$^{tm1.1Bird}$/Y mice showed an increase in the amounts of cholesterol intermediates, particularly desmosterol, toward wild-type levels at P70 (**Fig. 5f**,**g** and **Supplementary Table 3a**). The cholesterol biosynthesis pathway is inhibited in brains of *Mecp2*-null mice, probably because aberrant turnover results in cholesterol accumulation[33]. Treatment starting at an early age may therefore maintain some amount of pathway activity in the brain to increase lifespan and ameliorate motor symptoms in *Mecp2* mutant mice.

To determine whether the effects of fluvastatin were shared by other statin drugs, we treated 129.*Mecp2*$^{tm1.1Bird}$/Y mice with lovastatin, which differs from fluvastatin in its hydrophobicity, pharmacokinetics, transport and metabolism[37,38]. Lovastatin was of particular interest because it is highly lipophilic, increasing the likelihood that it will reach the brain. Lovastatin also ameliorates neurological symptoms in mouse models of fragile X syndrome[39] and is being used in clinical trials to ameliorate cognitive problems in children with neurofibromatosis type I[40]. Similarly to the fluvastatin dosing regimen, we began lovastatin treatment of 129.*Mecp2*$^{tm1.1Bird}$/Y mutant mice at 5 weeks of age, but we administered the mice a twice weekly dose of 1.5 mg per kg body weight throughout the trial (**Supplementary Table 5**). Lovastatin was also successful at ameliorating motor symptoms, as assessed by rotarod performance and open-field activity (**Fig. 5b**,**c** and **Supplementary Video 1**). Treatment with either statin drug at ten times the effective dose, however, was detrimental (**Supplementary Fig. 9**).

Statin drugs regulate systemic cholesterol through two mechanisms: inhibiting HMGCR and modifying liver uptake of serum LDL and triglycerides[38]. Notably, livers of 129.*Mecp2*$^{tm1.1Bird}$/Y mice had 39% higher lipid content per gram of tissue compared to wild-type littermates at P70 (**Fig. 5e**). These data suggest that systemic dyslipidemia resulted in increased accumulation of fat in the liver during the course of disease. Statin treatment not only decreased serum cholesterol concentrations in 129.*Mecp2*$^{tm1.1Bird}$/Y mice (**Fig. 5d**) but also successfully ameliorated the accumulation of lipids in the liver (**Fig. 5e**). Decreased fat accumulation probably occurs through the established effect of statins on liver LDL uptake[38].

To evaluate the effects of statin in mice that more closely model the predominantly female patients with RTT, we treated cohorts of 129.*Mecp2*$^{tm1.1Bird}$/+ female mice with a single dose of 3 mg per kg body weight fluvastatin weekly from P42 until 8 months of age (**Fig. 6** and **Supplementary Table 5**). The milder treatment regimen for female mice reflects their delayed onset of behavioral symptoms, as well as their lack of high serum cholesterol concentrations early in life (**Supplementary Fig. 10**). Motor performance assessed by rotarod at 5 months of age improved significantly ($P = 0.001$), and all treated mice lived for the length of the trial (**Fig. 6a**–**c**). Notably, the livers of female 129.*Mecp2*$^{tm1.1Bird}$/+ mice had 164% higher lipid content per gram of tissue than those of wild-type littermates at 8 months of age, which is a substantial increase (**Fig. 6e**). Notably, although serum cholesterol concentrations were unchanged, fluvastatin treatment reduced lipid accumulation in the liver to wild-type levels in female mice assessed at the end of the 8-month trial (**Fig. 6d**,**e**).

DISCUSSION

Our data show that cholesterol metabolism is abnormal in mouse models of RTT and that genetic and pharmacologic interventions to lower cholesterol synthesis lead to improvements in symptoms. Given the diverse roles of cholesterol in the nervous system, including membrane trafficking, signal transduction, myelin formation, dendrite remodeling, neuropeptide formation and synaptogenesis[33], abnormal brain cholesterol metabolism may be a crucial link between loss of MECP2 function and neuronal and glial dysfunction. Even small perturbations of cholesterol metabolism can have large effects on neuronal function, disrupting normal development[41,42] and contributing to aging disorders, including Huntington and Alzheimer diseases[43]. Within a fixed window of time, it is probable that cholesterol synthesis in the brain varies among cell types, including neuronal subtypes in various states of differentiation and activity, as well as among non-neuronal cells, including astrocytes, oligodendrocytes and microglia. Whole-brain cholesterol synthesis was decreased in *Mecp2*-null mice by 23% per gram of tissue, a notable difference considering the variety of cell types present. The only other mouse mutant to show decreased brain cholesterol synthesis is the *Cyp46a1* mutant mouse,

which lacks the 24S-hydroxycholesterol that is required for brain cholesterol turnover[44]. The discovery that re-expression of *Mecp2* in astrocytes contributes to the mitigation of RTT symptoms in a non–cell autonomous manner may be linked to cholesterol turnover, as astrocytes supplement neuronal cholesterol through lipoprotein transfer[45,46]. Cholesterol turnover is also required to produce geranylgeraniol, a product of HMGCR upstream of SQLE that is essential for learning and synaptic plasticity[31], and is important for the interaction between neurons and astrocytes at the synapse[28]. Furthermore, microglia, which function as brain macrophages, recycle neuronal cholesterol during dendrite pruning[47]; replacing mutant with wild-type microglia through bone-marrow transfer ameliorates RTT symptoms in *Mecp2*-null mice[14]. Modulating cholesterol homeostasis and turnover in the brain also ameliorates motor symptoms in *Mecp2*-null mice: fluvastatin treatment affects the abundance of desmosterol, which is produced primarily by astrocytes in the adult brain[33].

Perturbed lipid metabolism is evident in the livers as well as the brains of 129.*Mecp2*$^{tm1.1Bird}$ mice and is ameliorated by statin treatment. The precise mechanisms by which statin drugs alter brain cholesterol are unknown but probably include indirect effects of altered systemic lipid metabolism[48,49]. The *Sqle*^{Sum3Jus}/+ mutation in the 129.*Mecp2*$^{tm1.1Bird}$/Y genetic background rescued similar behavioral abnormalities as did statin treatment, although it did not change peripheral cholesterol concentrations. Furthermore, 129.*Mecp2*$^{tm1.1Bird}$/Y; *Sqle*^{Sum3Jus}/+ brains showed different patterns of sterol changes than did those of statin-treated mice. Statins affect pathways upstream of cholesterol synthesis and are indiscriminate of cell type, whereas the effect of SQLE is limited to cholesterol synthesis in a subset of neurons and glial cells. Notably, statin treatment improved behavioral parameters better than the mutation on this genetic background, raising the idea that modifiers may point to a targetable pathway without providing the most effective rescue.

Dysregulation of cholesterol homeostasis in the brain occurs concomitantly with symptom onset in *Mecp2*-null mice; however, male null and female heterozygous *Mecp2* mutant mice eventually accumulate fat in their livers. This fat accumulation is a sign of perturbed metabolism that can lead to fatty liver disease (FLD) when hepatic lipid accumulation is followed by an increase in oxidative and metabolic stress[50]. Thus, metabolic changes could exacerbate symptoms in *Mecp2* mutant mice, although pinpointing the cause of peripheral dyslipidemia will need to be a future endeavor, as conditional mutation of *Mecp2* by *Sim1*-Cre results in a subset of *Mecp2*-null symptoms that affect metabolism through the dysregulation of neuroendocrine pathways[51]. B6.*Mecp2*$^{tm1.1Jae}$/Y mice showed perturbations in brain lipid metabolism, even though they did not show systemic evidence of high cholesterol. Further, 129.*Mecp2*$^{tm1.1Bird}$/+ female mice accumulated large amounts of lipids in the liver yet showed only mildly elevated serum cholesterol and triglyceride concentrations. Lipid homeostasis is controlled by an interplay of multiple organ systems at many levels of feedback; therefore, it is probable that alleles and genetic background have a role in the full phenotypic outcome of disrupted lipid homeostasis that we uncovered in this genetic screen. However, our data suggest that altering brain cholesterol metabolism in *Mecp2* mutants is essential to improvements in motor function and longevity. A full understanding of lipid homeostasis in all organs of *Mecp2*-null mice, including muscle and the gastrointestinal systems, remains to be uncovered. Sterols are the precursors of steroid hormones, bile acids and vitamin D; thus, perturbations in lipid homeostasis may influence both neurological and non-neurological RTT symptoms, including abnormal responses to stress, high anxiety and bone anomalies[52]. The genetic and pharmacologic amelioration of brain and liver cholesterol perturbation suggests that downstream consequences of loss of *Mecp2* contribute to progressively worsening stages in disease pathology and should be considered when evaluating patients. Even so, our data suggest that peripheral dyslipidemia could be a biomarker in only a subset of patients with RTT.

A subset of *MECP2* missense mutations abolish interactions with a transcriptional co-repressor complex containing HDAC3, NCOR1, NCOR2 (also known as SMRT) and TBL1XR1 (also known as TBLR1). Such mutations recapitulate RTT phenotypes in mice and suggest that RTT dysfunction is caused by a failure of MECP2 to anchor the HDAC3-NCOR-SMRT complex to chromatin[53,54]. FLD in 129.*Mecp2*$^{tm1.1Bird}$ mice is similar to that in mice with liver-specific knockout of HDAC3 (refs. 55,56). HDAC3 regulates lipid homeostasis, and its loss in liver cells leads to metabolic syndrome and FLD[56,57]. Notably, the promoter regions of lipid and/or cholesterol homeostasis genes, including *Sqle*, seem to be targets of HDAC3 in the liver[55]. Our data support the idea that a MECP2-associated repressor complex such as the one containing HDAC3 may perform additional roles in regulating lipid homeostasis genes such as *Sqle* in the brain.

Screens for disease suppression have the potential to transform translational biology by identifying unrecognized pathways of pathogenesis, which would facilitate the rational design of new therapeutic strategies. Here we carried out a suppressor screen in mice that identified an unanticipated role for cholesterol biosynthesis in RTT disease pathology, a finding that is supported by the amelioration of symptoms in *Mecp2*-null mice after statin treatment. These data suggest that a subset of patients with RTT may be aided by pharmacological interventions that are designed to modulate lipid metabolism. Notably, moderate amounts of statin drugs were effective, whereas large doses were detrimental, demonstrating the importance of further studies to optimize treatment protocols. Although these findings do not comprise a preclinical trial, they point to mechanism-based strategies for treatment that may ameliorate a subset of symptoms and thereby improve quality of life for some patients with RTT. None of the suppressors eliminated symptoms entirely, supporting the idea that combination therapy will be required for thorough alleviation of RTT symptoms. The identification of additional suppressor loci may point to other potential targets.

METHODS

Methods and any associated references are available in the online version of the paper.

Note: Any Supplementary Information and Source Data files are available in the online version of the paper.

ACKNOWLEDGMENTS

The Genetics Analysis Facility (T. Patton and C. Marshall) at the Centre for Applied Genomics, Toronto Hospital for Sick Kids, Toronto, Ontario, Canada performed the Illumina Goldengate SNP analysis. We thank J. Crowe, M. Schrock, J. Borkey, M. Hill, A. Willis and J. Shaw (Justice laboratory), C. Lee, A. MacKenzie and L. Felker (Shendure laboratory), I. Adams (Katz laboratory), B. Thompson (McDonald and Russell laboratory) and K.S. Posey and A.M. Lopez (Turley laboratory) for technical assistance. We thank C. Spencer and R. Paylor for advice on assessing mouse behavior, which was carried out in the Baylor College of Medicine (BCM) Mouse Neurobehavior Core, and C. Reynolds for advice on plethysmography, which was carried out in the BCM Mouse Phenotyping Core. We thank H. Zoghbi and J. Neul (BCM) for *Mecp2* mutant mice. We also thank H. Zoghbi (BCM) and R. Behringer (University of Texas MD Anderson Cancer Center) for valuable discussions during revision of the manuscript. M. Coenraads of the Rett Syndrome Research Trust (RSRT) provided crucial moral and uninterrupted financial support while she aided intellectually through literature searches and advice.

The work was supported by grants from the RSRT, the Rett Syndrome Research Foundation, the International Rett Syndrome Foundation (ANGEL award 2608 to M.J.J. and ANGEL award 2583 to D.M.K.), Autism Science Foundation predoctoral fellowship #11-1015, US National Institutes of Health (NIH) grants NIH T32 GM08307 to C.M.B., NIH U54 GM69338 to D.W.R., NIH R01 HL09610 to S.D.T. and NIH R01 CA115503 to M.J.J. and the National Institute of Neurologic Diseases

and Stroke, including funding from the American Recovery and Reinvestment Act (D.M.K.). Grants to the BCM Diabetes and Endocrinology Research Center (2P30DK079638-05) and the BCM Intellectual and Developmental Disabilities Research Center (5P30HD024064-23) from the NIH Eunice Kennedy Shriver National Institute of Child Health and Human Development also supported this work. The content is solely the responsibility of the authors and does not necessarily represent the official views of the Eunice Kennedy Shriver National Institute of Child Health and Human Development or the NIH.

AUTHOR CONTRIBUTIONS

M.J.J. conceived of the work, carried out the genetic screen and dissected embryos. J.S. and W.H. carried out the capture sequencing and analysis. C.M.B. confirmed map locations and lesions, performed statin injections and carried out behavior and plethysmography testing and quantitative RT-PCR (qRT-PCR). S.M.K. performed protein blotting and liver histopathology. H.M.B. performed preliminary qRT-PCR. J.G.M., B.L. and S.D.T. analyzed sterols and performed synthesis studies. S.D.T. evaluated liver cholesterol and triglycerides. A.A.P. and D.M.K. provided Jaenisch mice and laboratory facilities. D.M.K. helped analyze plethysmography data. M.J.J., D.W.R., D.M.K., S.D.T., S.M.K. and C.M.B. wrote the manuscript with input from the other coauthors.

COMPETING FINANCIAL INTERESTS

The authors declare no competing financial interests.

1. Amir, R.E. *et al.* Rett syndrome is caused by mutations in X-linked *MECP2*, encoding methyl-CpG–binding protein 2. *Nat. Genet.* **23**, 185–188 (1999).
2. Bienvenu, T. & Chelly, J. Molecular genetics of Rett syndrome: when DNA methylation goes unrecognized. *Natl. Rev. Genet.* **7**, 415–426 (2006).
3. Guy, J., Hendrich, B., Holmes, M., Martin, J.E. & Bird, A. A mouse *Mecp2*-null mutation causes neurological symptoms that mimic Rett syndrome. *Nat. Genet.* **27**, 322–326 (2001).
4. Shepherd, G.M. & Katz, D.M. Synaptic microcircuit dysfunction in genetic models of neurodevelopmental disorders: focus on Mecp2 and Met. *Curr. Opin. Neurobiol.* **21**, 827–833 (2011).
5. Kavalali, E.T., Nelson, E.D. & Monteggia, L.M. Role of MeCP2, DNA methylation, and HDACs in regulating synapse function. *J. Neurodev. Disord.* **3**, 250–256 (2011).
6. Guy, J., Gan, J., Selfridge, J., Cobb, S. & Bird, A. Reversal of neurological defects in a mouse model of Rett syndrome. *Science* **315**, 1143–1147 (2007).
7. Collins, A.L. *et al.* Mild overexpression of MeCP2 causes a progressive neurological disorder in mice. *Hum. Mol. Genet.* **13**, 2679–2689 (2004).
8. Chahrour, M. *et al.* MeCP2, a key contributor to neurological disease, activates and represses transcription. *Science* **320**, 1224–1229 (2008).
9. Stancheva, I., Collins, A.L., Van den Veyver, I.B., Zoghbi, H. & Meehan, R.R. A mutant form of MeCP2 protein associated with human Rett syndrome cannot be displaced from methylated DNA by notch in *Xenopus* embryos. *Mol. Cell* **12**, 425–435 (2003).
10. St Johnston, D. The art and design of genetic screens: *Drosophila melanogaster*. *Nature Rev. Genet.* **3**, 176–188 (2002).
11. Carpinelli, M.R. *et al.* Suppressor screen in *Mpl–/–* mice: c-Myb mutation causes supraphysiological production of platelets in the absence of thrombopoietin signaling. *Proc. Natl. Acad. Sci. USA* **101**, 6553–6558 (2004).
12. Matera, I. *et al.* A sensitized mutagenesis screen identifies Gli3 as a modifier of Sox10 neurocristopathy. *Hum. Mol. Genet.* **17**, 2118–2131 (2008).
13. Justice, M.J., Siracusa, L.D. & Stewart, A.F. Technical approaches for mouse models of human disease. *Dis. Model. Mech.* **4**, 305–310 (2011).
14. Derecki, N.C. *et al.* Wild-type microglia arrest pathology in a mouse model of Rett syndrome. *Nature* **484**, 105–109 (2012).
15. Neuhaus, I.M. & Beier, D.R. Efficient localization of mutations by interval haplotype analysis. *Mamm. Genome* **9**, 150–154 (1998).
16. Moran, J.L. *et al.* Utilization of a whole genome SNP panel for efficient genetic mapping in the mouse. *Genome Res.* **16**, 436–440 (2006).
17. Fairfield, H. *et al.* Mutation discovery in mice by whole exome sequencing. *Genome Biol.* **12**, R86 (2011).
18. Jurevics, H.A., Kidwai, F.Z. & Morell, P. Sources of cholesterol during development of the rat fetus and fetal organs. *J. Lipid Res.* **38**, 723–733 (1997).
19. Zlokovic, B.V. The blood-brain barrier in health and chronic neurodegenerative disorders. *Neuron* **57**, 178–201 (2008).
20. Gill, S., Stevenson, J., Kristiana, I. & Brown, A.J. Cholesterol-dependent degradation of squalene monooxygenase, a control point in cholesterol synthesis beyond HMG-CoA reductase. *Cell Metab.* **13**, 260–273 (2011).
21. Cory, E.J., Russey, W.E. & Ortiz de Montellano, P.R. 2,3-oxidosqualene, an intermediate in the biological synthesis of sterols from squalene. *J. Am. Chem. Soc.* **88**, 4750–4751 (1966).
22. Yamamoto, S. & Bloch, K. Studies on squalene epoxidase of rat liver. *J. Biol. Chem.* **245**, 1670–1674 (1970).
23. Shibata, N. *et al.* Supernatant protein factor, which stimulates the conversion of squalene to lanosterol, is a cytosolic squalene transfer protein and enhances cholesterol biosynthesis. *Proc. Natl. Acad. Sci. USA* **98**, 2244–2249 (2001).
24. Astruc, M., Tabacik, C., Descomps, B. & de Paulet, A.C. Squalene epoxidase and oxidosqualene lanosterol-cyclase activities in cholesterogenic and non-cholesterogenic tissues. *Biochim. Biophys. Acta* **487**, 204–211 (1977).
25. Ingham, P.W., Nakano, Y. & Seger, C. Mechanisms and functions of Hedgehog signalling across the metazoa. *Natl. Rev. Genet.* **12**, 393–406 (2011).
26. Posé, D. & Botella, M.A. Analysis of the *Arabidopsis* dry2/sqe1-5 mutant suggests a role for sterols in signaling. *Plant Signal. Behav.* **4**, 873–874 (2009).
27. Posé, D. *et al.* Identification of the *Arabidopsis* dry2/sqe1-5 mutant reveals a central role for sterols in drought tolerance and regulation of reactive oxygen species. *Plant J.* **59**, 63–76 (2009).
28. Nieweg, K., Schaller, H. & Pfrieger, F.W. Marked differences in cholesterol synthesis between neurons and glial cells from postnatal rats. *J. Neurochem.* **109**, 125–134 (2009).
29. Dietschy, J.M., Turley, S.D. & Spady, D.K. Role of liver in the maintenance of cholesterol and low density lipoprotein homeostasis in different animal species, including humans. *J. Lipid Res.* **34**, 1637–1659 (1993).
30. Dietschy, J.M. Central nervous system: cholesterol turnover, brain development and neurodegeneration. *Biol. Chem.* **390**, 287–293 (2009).
31. Russell, D.W., Halford, R.W., Ramirez, D.M., Shah, R. & Kotti, T. Cholesterol 24-hydroxylase: an enzyme of cholesterol turnover in the brain. *Annu. Rev. Biochem.* **78**, 1017–1040 (2009).
32. Chen, R.Z., Akbarian, S., Tudor, M. & Jaenisch, R. Deficiency of methyl-CpG binding protein-2 in CNS neurons results in a Rett-like phenotype in mice. *Nat. Genet.* **27**, 327–331 (2001).
33. Pfrieger, F.W. & Ungerer, N. Cholesterol metabolism in neurons and astrocytes. *Prog. Lipid Res.* **50**, 357–371 (2011).
34. Xie, C., Lund, E.G., Turley, S.D., Russell, D.W. & Dietschy, J.M. Quantitation of two pathways for cholesterol excretion from the brain in normal mice and mice with neurodegeneration. *J. Lipid Res.* **44**, 1780–1789 (2003).
35. Ko, M. *et al.* Cholesterol-mediated neurite outgrowth is differently regulated between cortical and hippocampal neurons. *J. Biol. Chem.* **280**, 42759–42765 (2005).
36. Jolley, C.D., Dietschy, J.M. & Turley, S.D. Genetic differences in cholesterol absorption in 129/Sv and C57BL/6 mice: effect on cholesterol responsiveness. *Am. J. Physiol.* **276**, G1117–G1124 (1999).
37. Bellosta, S., Paoletti, R. & Corsini, A. Safety of statins: focus on clinical pharmacokinetics and drug interactions. *Circulation* **109**, III50–III57 (2004).
38. García-Sabina, A., Gulin-Davila, J., Sempere-Serrano, P., Gonzalez-Juanatey, C. & Martinez-Pacheco, R. Specific considerations on the prescription and therapeutic interchange of statins. *Farm. Hosp.* **36**, 97–108 (2012).
39. Osterweil, E.K. *et al.* Lovastatin corrects excess protein synthesis and prevents epileptogenesis in a mouse model of fragile X syndrome. *Neuron* **77**, 243–250 (2013).
40. Ardern-Holmes, S.L. & North, K.N. Therapeutics for childhood neurofibromatosis type 1 and type 2. *Curr. Treat. Options Neurol.* **13**, 529–543 (2011).
41. Keber, R. *et al.* Mouse knockout of the cholesterogenic cytochrome P450 lanosterol 14α-demethylase (Cyp51) resembles Antley-Bixler syndrome. *J. Biol. Chem.* **286**, 29086–29097 (2011).
42. Waterham, H.R. Defects of cholesterol biosynthesis. *FEBS Lett.* **580**, 5442–5449 (2006).
43. Björkhem, I. & Hansson, M. Cerebrotendinous xanthomatosis: an inborn error in bile acid synthesis with defined mutations but still a challenge. *Biochem. Biophys. Res. Commun.* **396**, 46–49 (2010).
44. Lund, E.G. *et al.* Knockout of the cholesterol 24-hydroxylase gene in mice reveals a brain-specific mechanism of cholesterol turnover. *J. Biol. Chem.* **278**, 22980–22988 (2003).
45. Lioy, D.T. *et al.* A role for glia in the progression of Rett's syndrome. *Nature* **475**, 497–500 (2011).
46. Vance, J.E. Dysregulation of cholesterol balance in the brain: contribution to neurodegenerative diseases. *Dis. Model. Mech.* **5**, 746–755 (2012).
47. Paolicelli, R.C. *et al.* Synaptic pruning by microglia is necessary for normal brain development. *Science* **333**, 1456–1458 (2011).
48. Cibičkova, L. Statins and their influence on brain cholesterol. *J. Clin. Lipidol.* **5**, 373–379 (2011).
49. Stranahan, A.M., Cutler, R.G., Button, C., Telljohann, R. & Mattson, M.P. Diet-induced elevations in serum cholesterol are associated with alterations in hippocampal lipid metabolism and increased oxidative stress. *J. Neurochem.* **118**, 611–615 (2011).
50. Day, C.P. & James, O.F. Steatohepatitis: a tale of two "hits?". *Gastroenterology* **114**, 842–845 (1998).
51. Fyffe, S.L. *et al.* Deletion of Mecp2 in Sim1-expressing neurons reveals a critical role for MeCP2 in feeding behavior, aggression, and the response to stress. *Neuron* **59**, 947–958 (2008).
52. Percy, A.K. Rett syndrome: exploring the autism link. *Arch. Neurol.* **68**, 985–989 (2011).
53. Lyst, M.J. *et al.* Rett syndrome mutations abolish the interaction of MeCP2 with the NCoR/SMRT transcriptional co-repressor. *Nat. Neurosci.* **16**, 898–902 (2013).
54. Ebert, D.H. *et al.* Activity-dependent phosphorylation of MECP2 threonine 308 regulates interaction with NcoR. *Nature* published online; doi:10.1038/nature12348 (16 June 2013).
55. Knutson, S.K. *et al.* Liver-specific deletion of histone deacetylase 3 disrupts metabolic transcriptional networks. *EMBO J.* **27**, 1017–1028 (2008).
56. Sun, Z. *et al.* Hepatic Hdac3 promotes gluconeogenesis by repressing lipid synthesis and sequestration. *Nat. Med.* **18**, 934–942 (2012).
57. Feng, D. *et al.* A circadian rhythm orchestrated by histone deacetylase 3 controls hepatic lipid metabolism. *Science* **331**, 1315–1319 (2011).

ONLINE METHODS

Mouse strains and genetic screen. All animal experiments were conducted under protocols approved by local Animal Care and Use Committees in Association for Assessment and Accreditation of Laboratory Animal Care International (AAALAC)-accredited animal facilities at BCM and the University of Texas Southwestern. Congenic 129.*Mecp2*$^{tm1.1Bird}$/+ female mice were maintained by backcrossing females to males of the 129S6/SvEvTac strain. C57BL/6J males were imported from The Jackson Laboratory at 6 weeks of age and injected with three weekly doses of 100 mg per kg body weight ENU at 8 weeks of age as described[58]. After recovery of fertility, 60 ENU-treated males were mated to 129.*Mecp2*$^{tm1.1Bird}$/+ females, and their G_1 male offspring were genotyped for *Mecp2* allele status according to The Jackson Laboratory standard protocols. The B6.*Mecp2*$^{tm1.1Jae}$ line was made in a hybrid 129/Ola C57BL/6 embryonic stem cell line[32] and backcrossed to C57BL/6J for over ten generations. The line is maintained by additional backcrosses to C57BL/6J mice.

For each founder line, long-lived G_1 males were mated to 129S6/SvEvTac females; G_2 offspring were mated to 129.*Mecp2*$^{tm1.1Bird}$/+ females or 129S6/SvEvTac males to produce N_3 mice for linkage mapping. Fine structure mapping was achieved with informative MIT markers identified using the Mouse Genome Informatics website (http://www.informatics.jax.org). PCR (ABI) followed by gel electrophoresis with MetaPhor agarose (Lonza) on relevant primer pairs determined whether a given mouse carried heterozygous B6/129S6 or 129S6 homozygous DNA at each locus of interest. Primers are available upon request.

The investigator is blind to genetic mutation status when phenotyping in a forward genetic screen. Once a map location was found, mice were genotyped after the fact to find that the rescue phenotype correlated with the genotype.

Lipid and sterol analyses. 129.*Mecp2*$^{tm1.1Bird}$/Y mice and age-matched +/Y littermate controls housed in plastic Lab Products cages with corncob bedding in rooms with alternating 13-h and 11-h periods of light and dark, respectively, were provided with acidified water and a Harlan Teklad 2920X diet *ad libitum* (19.1% protein, 6.5% fat, 0% cholesterol). Gene expression, serum cholesterol concentrations (Cobas Mira clinical chemistry analyzer) and tissue lipids were assessed within a 2-h afternoon window after a 4–6 h fast at P28 and P56. Brain analyses were performed on the subcortical region, which contains the corpus callosum, striatum, thalamus, hypothalamus and hippocampus. Cholesterol intermediates were measured by tandem mass spectrometry following a previously published protocol[59] after extraction from tissue of mice treated as described above. Before gas-liquid chromatography, lipids were isolated from tissue using $CHCl_3$:CH_3OH extraction, followed by drying of the organic phase under N_2 pressure. Tissue cholesterol concentrations were assessed by gas-liquid chromatography, and cholesterol synthesis was assessed from saponified tissue after the incorporation of 100 mCi ^3H_2O after intraperitoneal injection as described[34]. For the *in vivo* cholesterol synthesis study, samples were obtained from mice in a fed state the late dark phase of a 12-h on/off light/dark cycle. These mice were adapted to individual housing and a Harlan Teklad 7001 rodent chow (low cholesterol (0.02%, wt/wt), low fat (4% wt/wt)) starting at P38 before analysis. The age of mice at sampling was P54–P56. All chemical assays were performed blinded to genotype and treatment group.

Real-time RT-PCR. Brain RNA was isolated using an RNeasy Lipid Tissue Mini Kit (Qiagen), and liver RNA was isolated using Trizol (Invitrogen) according to the manufacturer's instructions. Liver RNA was treated with 1 IU DNase (Ambion Inc.) at 37 °C for 1 h per the manufacturer's instructions. First-strand cDNA was synthesized from 5,000 ng of total RNA using the SuperScript III First-Strand Synthesis System (Invitrogen) per the manufacturer's instructions. RT-PCR was performed in triplicate for each sample on an ABI 7900 instrument (Applied Biosystems, CA, USA). Gene primers for qRT-PCR were designed against published mRNA sequences using Primer3 software and synthesized by Integrated DNA Technologies (Iowa, USA). Primer sequences are available by request. qRT-PCR was performed in triplicate on an ABI 7900 instrument (Applied Biosystems, CA, USA). Reactions contained cDNA from 10 ng total RNA, 0.1 µl forward and reverse primers, 5 µl Power SYBR Green Master Mix and water to a final volume of 10 µl. The PCR conditions were as follows: 95 °C for 10 min, 40 cycles of 95 °C for 15 s and 60 °C for 60 s. Single-product amplification was confirmed by disassociation curves and agarose gel electrophoresis. Gene expression was normalized to an *RpL19* (also known as *L19*) internal loading control, analyzed using the $2^{-(\Delta\Delta CT)}$ method and expressed as either a raw $2^{-(\Delta\Delta CT)}$ value or the expression in *Mecp2*/Y mice relative to that in wild-type mice[60].

Exome sequencing. Genomic DNA was isolated from two N_3 cousin offspring of two N_2 mice (female 5 and female 8) from line 895 (*Sum3*^{m1Jus}) and from C57BL/6J and 129S6/SvEvTac mice by standard methods. Mouse exome-capture reagents were designed to a 54.3-Mb target, including 203,225 exonic regions (C57BL/6J, NCBI37/mm9)[17]. Sequencing of post-enrichment shotgun libraries was performed on an Illumina GA2x (paired-end, 76-bp reads) or Illumina HiSeq 2000 (paired-end, 100-bp reads). Sequence reads were mapped to the mm9 reference genome with BWA[61], and variants were called with SAMtools[62] requiring a minimum SNP quality of 20. Custom scripts were used to annotate variants with respect to their predicted impact on protein sequence. To remove inbred strain polymorphisms as well as systematic sequencing artifacts, variants were removed from consideration if they were identified in any of 15 other mouse strains (including the parental strains, which were resequenced alongside the mutants), other lines from this study or other phenotypes.

Drug administration. Fluvastatin (Selleckchem) was dissolved in sterile ultrapure water such that the desired dose for a 20 g mouse was given in 100 µl and was administered subcutaneously. Male mice were given a single 3 mg per kg body weight weekly dose at 5, 6 and 7 weeks of age and were then given three times weekly (Monday, Wednesday and Friday) 3 mg per kg body weight doses beginning at 8 weeks of age. Female mice also received 3 mg per kg body weight doses but were treated only once per week beginning at 6 weeks of age. Lovastatin (Tocris Bioscience) preparation required activation in ethanol followed by adjustment to pH 7.2, as per the product information guidelines. The activated stock solution was diluted with ethanol to 20× the injected dose and kept at −20 °C for up to 1 month. The day of injection, a 1× working solution was prepared by diluting the stock solution in sterile saline such that the desired dose for a 20 g mouse was given in 100 µl. Male mice were injected subcutaneously with a twice-weekly 1.5 mg per kg body weight dose beginning at 5 weeks of age. The precise timing of the injections and phenotyping assays can be found in **Supplementary Table 5**.

For each of the two types of statin treatment, littermates of the same genotype were divided between the treatment and control groups such that the average and s.d. of the starting weights and subjective health scores of the two groups were statistically indistinguishable. Cohorts of mixed genotypes in sample sizes of 10 per group were treated and assessed independently to ensure randomization and repeatability.

Assessments of behavior and breathing. Open-field locomotor activity was assessed using Versamax Animal Activity Monitors. Recordings were taken in a secluded room with dim light (20–25 lx) and artificial white noise (55–60 dB). Each mouse was placed in the center of the open-field chamber, and activity was recorded for 30 min. An aspect of motor performance was measured using the accelerating rotating rod (rotarod) (Stoelting). At 8 weeks (males) or 12 weeks (females) of age, mice were placed on a grooved rod rotating at a speed of 4 r.p.m. Over the course of a 5-min trial, the revolution rate increased steadily to a maximum of 40 r.p.m. The time each mouse was able to stay on the rod was recorded for eight trials, four on each of 2 consecutive days, with a minimum of 30 min between trials. A trial ended when the mouse fell off the rod, spun with the rod for two consecutive revolutions or successfully stayed on the rod for 5 min. Pre-pulse inhibition was measured using SR-Lab Startle Chambers (San Diego Instruments). Unrestrained, whole-body plethysmography was carried out using the Buxco FinePointe system. Breathing parameters were recorded for 1 h after a 30-min acclimation period. Mice were monitored for activity. The data represent breathing during periods of stillness.

For fluvastatin treatment, subsequent to the pilot study that included 6 *Mecp2*-null mice per treatment group, all behavioral assessments were performed with the experimenter blinded to treatment group. For lovastatin treatment, all behavioral assessments were performed blinded to treatment group. For studies of the *Sqle*^{Sum3Jus} line, although genotype information was obtained before the start of behavioral studies to ensure equal numbers

of each genotype were being assayed, this information was not linked to the mice until all behavioral assays were complete.

Statistics. LOD scores were generated using the R/qtl statistics package[63]. Survival curves were compared using SPSS by Kaplan-Meier analysis followed by log-rank comparison. Statistical comparisons between two groups (wild-type mice compared to *Mecp2* mutants) were performed in GraphPad Prism 5 using an unpaired, two-tailed Student's *t* test; equal variances were not assumed, as the *Mecp2* mutant group typically showed increased variability compared to the wild-type group. Statistical tests requiring multiple comparisons were analyzed in SPSS. Excepting the rotarod data, comparisons between multiple groups were analyzed by one-way ANOVA, and sphericity was not assumed; the Bonferroni adjustment was applied when comparing more than two genotypes, and the Dunnett *post-hoc* test was used to compare statin-treated groups with the vehicle-treated control group. Rotarod data were analyzed using repeated measures ANOVA.

For behavioral assays, sample sizes of at least 12 mice per group are recommended for preclinical assays. For chemical assays, samples sizes of 4–6 per group are usually sufficient to see significant differences. For the suppressor screen, we chose to screen one genome's equivalent—approximately 700 gametes, when ENU is expected to produce one new mutation in a single gene in every 700 gametes screened. qPCR data were the only data in which outliers were observed. An outlier in triplicate repeats of a single sample was excluded if it was ≥2 s.d. above the mean for a given group.

58. Kile, B.T. *et al.* Functional genetic analysis of mouse chromosome 11. *Nature* **425**, 81–86 (2003).
59. McDonald, J.G., Smith, D.D., Stiles, A.R. & Russell, D.W. A comprehensive method for extraction and quantitative analysis of sterols and secosteroids from human plasma. *J. Lipid Res.* **53**, 1399–1409 (2012).
60. Livak, K.J. & Schmittgen, T.D. Analysis of relative gene expression data using real-time quantitative PCR and the 2–ΔΔC(T) method. *Methods* **25**, 402–408 (2001).
61. Li, H. & Durbin, R. Fast and accurate long-read alignment with Burrows-Wheeler transform. *Bioinformatics* **26**, 589–595 (2010).
62. Li, H. *et al.* The Sequence Alignment/Map format and SAMtools. *Bioinformatics* **25**, 2078–2079 (2009).
63. Broman, K.W., Wu, H., Sen, S. & Churchill, G.A. R/qtl: QTL mapping in experimental crosses. *Bioinformatics* **19**, 889–890 (2003).